Electronic Supplementary Information

Acid-base resistant ligand-modified molybdenum-sulfur clusters with enhanced photocatalytic activity towards hydrogen evolution

Hui-Li Zheng,[a,b] Jian-Qiang Zhao,[a] Jian Zhang,*[a] and Qipu Lin*[a]

[a] *State Key Laboratory of Structural Chemistry, Fujian Institute of Research on the Structure of Matter, Chinese Academy of Sciences, Fuzhou, Fujian 350002, China.*

E-mail: linqipu@fjirsm.ac.cn, zhj@fjirsm.ac.cn

[b] *University of Chinese Academy of Sciences, Beijing 100049, China.*

Table of Contents	
Experimental	Synthetic procedure and equipment.
Figure S1	The relationship of the [Mo_3S_7] SBUs to the monolayer MoS_2 with sulfur-rich edges.
Figure S2	The PXRD patterns of simulated and experiment of $(NEt_4)_2Mo^{IV}{}_3S_7Br_6$.
Figure S3	(a) The crystal structure of compound MoS-MBTZ by side and top view; (b) The packing diagrams of compound MoS-MBTZ in the view of a-axis, b-axis and c-axis.
Figure S4	Summary of compounds with trinuclear [Mo_3S_7] SBUs.
Figure S5	The PXRD patterns of simulated, MoS-MBTZ bulk crystal and MoS-MBTZ microscale crystal.
Figure S6	The TGA curve of MoS-MBTZ.
Figure S7	The high-resolution XPS spectra of Mo 3*d* of compound MoS-MBTZ.
Figure S8	The experimental and calculated ESI-MS spectra of MoS-MBTZ.
Figure S9	UV-vis absorption spectra of MoS-MBTZ and MoS-Br.
Figure S10	Photocatalytic H_2 evolution from a mixed solution of organic solvent and H_2O at a volume ratio of 9:1.
Figure S11	Photocatalytic H_2 evolution from a mixed solution of CH_3CN and H_2O at different volume ratio.
Figure S12	Photocatalytic H_2 evolution from a mixed solution of CH_3CN and H_2O at a volume ratio of 9:1with different electron donor.
Figure S13	Photocatalytic H_2 evolution of MoS-MBTZ in recycling experiments.
Figure S14	The XRD of MoS-MBTZ before and after photocatalysis.
Figure S15	The SEM image of MoS-MBTZ before and after photocatalysis.
Figure S16	The FT-IR of MoS-MBTZ before and after photocatalysis.
Figure S17	The XPS image of MoS-MBTZ before and after photocatalysis.
Figure S18	The ESI-MS of MoS-MBTZ before and after photocatalysis.
Figure S19	Photocatalytic H_2 evolution of MoS-MBTZ after soaking in different pH solutions for one month.
Figure S20	The steady-state fluorescence spectra of $[Ru(bpy)_3]Cl_2$ upon the addition of increasing amounts of TEOA in the CH_3CN/H_2O solution.
Figure S21	The steady-state fluorescence spectra of $[Ru(bpy)_3]Cl_2$ upon the addition of increasing amounts of MoS-Br in the CH_3CN/H_2O solution.
Figure S22	The EIS Nyquist plots for MoS-MBTZ and MoS-Br.
Figure S23	The molecular orbitals of HOMO (a) and LUMO (b) for MoS-Br.
Figure S24	The PDOS of Mo-4*d*, S-3*p* and Br-4*p* for MoS-Br.
Table S1	Crystal data and structure refinement for MoS-MBTZ.

Materials:

Precursor $(NEt_4)_2Mo_3S_7Br_6$ was synthesized by a reported procedure.[1] Other chemical reagents were obtained from commercial supply without further purification. 2-mercaptobenzothiazole (MBTZ, 99.8%, J&K), [Ru(2,2'-bipyridine)$_3$]$Cl_2 \cdot 6H_2O$ ([Ru(bpy)$_3$]Cl_2, 99%, Aladdin), N,N-dimethylformamide (DMF, 99%, Aladdin), ethyl acetate (99%, Aladdin), acetonitrile (MeCN, 99%, Aladdin), methanol (MeOH, 99%, Aladdin), triethanolamine (TEOA, 99%, Aladdin), tetrafluoroboric acid (HBF_4, 99%, Aladdin). Deionized water was generated by the Hitech purified water system.

Synthesis of block crystal of MoS-MBTZ:

The mixture of $(NEt_4)_2Mo_3S_7Br_6$ (125.1 mg, 0.1 mmol) and 2-mercaptobenzothiazole (54.3 mg, 0.3 mmol) were dissolved in 1 mL DMF and 2 mL ethyl acetate in a 20 mL glass vial. Three drops HBF_4 were added to the above solution and stirred for half an hour. Then, the mixture was heated at 100 °C for 48 h, followed by cooling to room temperature. Lots of orange needle crystals were filtrated from the vial and washed with ethanol three times (ca. 68% yield based on $(NEt_4)_2Mo_3S_7Br_6$). The structure was subsequently determined to be $Mo_3S_{13}BrC_{21}H_{12}N_3$ by using the single crystal X-ray diffraction. Elemental analysis calculated (%): C 23.12; H 1.11; N 3.85. Found (%): C 23.07; H 1.20; N 3.77. Selected IR (KBr pellet, cm^{-1}): ν (cm^{-1}) = 3440 (m), 3049 (w), 1587 (w), 1456 (m), 1386 (s), 1089 (s), 1039 (s), 1016 (m), 752 (s), 694 (w), 520 (w).

Synthesis of MoS-MBTZ microcrystal:

$(NEt_4)_2Mo_3S_7Br_6$ (125.1 mg, 0.1 mmol) and 2-mercaptobenzothiazole (54.3 mg, 0.3 mmol) were dissolved in 6 mL DMF and 12 mL ethyl acetate. Three drops of HBF_4 were added to the above solution. Then, the mixture was refluxed at 100 °C for 12 h. The orange microcrystals were obtained and confirmed by powder X-ray diffraction.

Characterizations:

Fourier transform infrared (FT-IR) spectra were recorded from KBr pellets containing 1% of the compound in the range of 400~4000 cm^{-1} on a Nicolet Magna 750 FT-IR spectrometer. Elemental analysis of C, H, N were performed on a Vario EL-Cube. Thermal gravimetric analysis (TGA) was carried out on a Netzsch STA449F3 thermal analyzer at a temperature range of 25 to 800 °C under N_2 atmosphere with a heating rate of 10 °C min^{-1}. Powder X-ray diffraction (PXRD) patterns of the samples were recorded by a Rigaku Dmax 2500 X-ray

diffractometer with Cu *K*α radiation (λ = 1.54056 Å). Scanning electron microscopy (SEM) images were obtained by a Zeiss Sigma 500. Surface chemical analyses were performed by X-ray photoelectron spectroscopy (XPS, Thermo Fisher, ESCALAB 250Xi). Ultraviolet-visible (UV-Vis) diffuse-reflectance spectra (DRS) were performed on a Shimadzu UV-1201PC spectrophotometer. Steady-state photoluminescence (PL) spectra and time-resolved PL decay spectra were performed on a FLS980 Spectrometer.

X-ray Crystallography:

The diffraction data sets were collected on a Bruker Smart Apex CCD diffractometer with graphite monochromatic Mo-*Kα* radiation (λ = 0.71073 Å) at 293 K. The structures were solved by direct methods and refined by full-matrix least-squares on F^2 using SHELXL-2014.[2] All non-hydrogen atoms were refined using anisotropic displacement parameters. The hydrogen atoms of the ligand were generated geometrically. The structure figures were produced by Diamond 4.0 software. Crystallographic details are provided in Table S1 and selected bond lengths and angles are listed in Table S2. The crystal structure of compound has been deposited and CCDC numbers are 2123562 for MoS-MBTZ.

Photocatalytic hydrogen evolution reactions:

The photocatalytic hydrogen production experiments were performed in a sealed Pyrex reactor (250 mL) with a top flat quartz window for light irradiation and a silicone rubber septum was fixed on its side for sampling produced H_2 in the headspace of reaction cell. Catalyst (5 mg) and $[Ru(bpy)_3]Cl_2$ (15 mg) were added into the mixed solution of CH_3CN/H_2O (9:1) containing 10% TEOA with magnetic stirring and the total amount of solution was 60mL. After degassing with N_2 to remove dissolved air for 20 min, the reaction was performed under the irradiation of a 300 W Xe lamp with UV and IR-cut to keep the wavelengths in the range from 420 to 800 nm. Keeping the reaction temperature at 298K by using the cooling water circulation. The generated gas products were analyzed by a gas chromatography analyzer (FULI 9790II) equipped with the thermal conductivity detector (TCD).

Photo/electrochemical measurements:

Mott-Schottky plots were measured on an IM 6 electrochemical system in 0.2 M Na_2SO_4 electrolyte at room temperature with Ag/AgCl electrode as the reference electrode and Pt plate as the counter electrode, at the frequencies of 500, 1000 and 1500 Hz. The electrochemical impedance spectra (EIS) and photocurrent tests were performed on the CHI660E

electrochemical workstation using a standard three-electrode system, consisting of an F-doped SnO_2 (FTO) electrode coated with photocatalyst, a Pt plate counter-electrode, and an Ag/AgCl reference electrode. Preparation of working electrodes: Sample (5 mg) were dispersed in the solution containing ethanol (0.5 mL), acetonitrile (0.5 mL) and Nafion (10 μL) then ultrasonication for 30 min. 20 μL of the prepared suspension was pipetted onto the FTO (0.25 cm^2) and dried at ambient temperature.

Electrospray Mass spectrometry measurement:

Electrospray ionization mass spectrometry (ESI-MS) measurements were conducted with a Thermo Exactive spectrometer in positive ion mode at a capillary temperature of 275 ^oC. The spectrometer was previously calibrated with the standard tune mix to give a precision of ca. 2 ppm in the region of 50-4000 m/z. Aliquots of the solution were injected into the device at 0.3 mL/h. The capillary voltage was 50 V, the tube lens voltage was 150 V and the skimmer voltage was 25 V. The in-source energy was set to 0-100 eV with a gas flow rate at 10 mL/min of the maximum. The mass spectrometry data was analyzed by the software of Thermo Foundation 4.0.

Theoretical band calculation:

The single crystal data of compounds MoS-MBTZ and MoS-Br were directly used to calculate the electronic band structure in Castep software. The total energy was calculated with density functional theory (DFT) using Perdew-Burke-Ernzerhof (PBE) generalized gradient approximation.[3] The interactions between the ionic cores and the electrons were described by the norm-conserving pseudopotential. Hence, the C-$2s^22p^2$, N-$2s^22p^3$, H-$1s^1$, Mo-$4d^55s^1$, S-$3s^23p^4$ and Br-$4s^24p^5$ orbital were adopted as valence electrons. The number of plane wave included in the basis sets was determined by a cutoff energy of 320 eV and numerical integration of the Brillouin zone is performed using Monkhorst-Pack k-point sampling of 2×2×2. Other calculating parameters and convergence criteria were set by the default values of the CASTEP code.

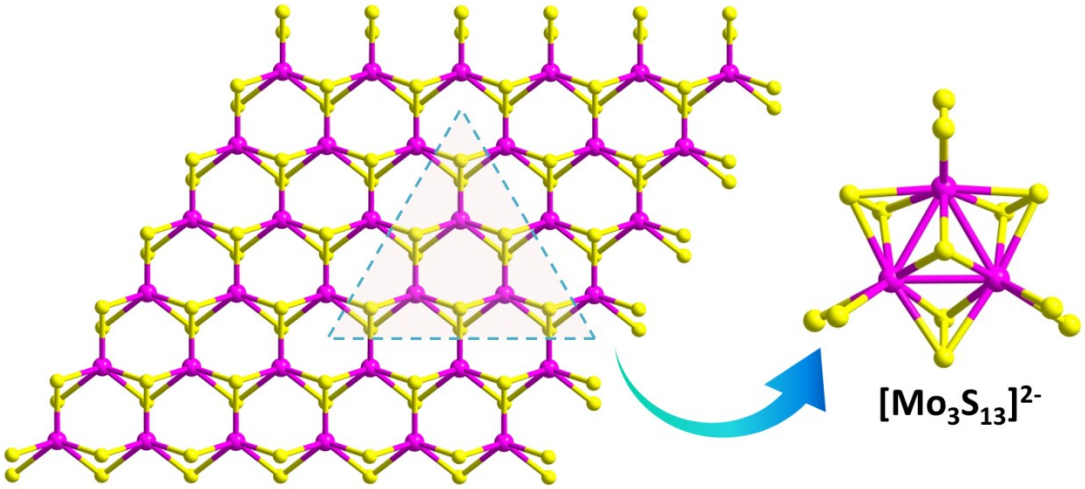

Fig. S1 The relationship of the $[Mo_3S_7]$ SBUs to the monolayer MoS_2 with sulfur-rich edges.

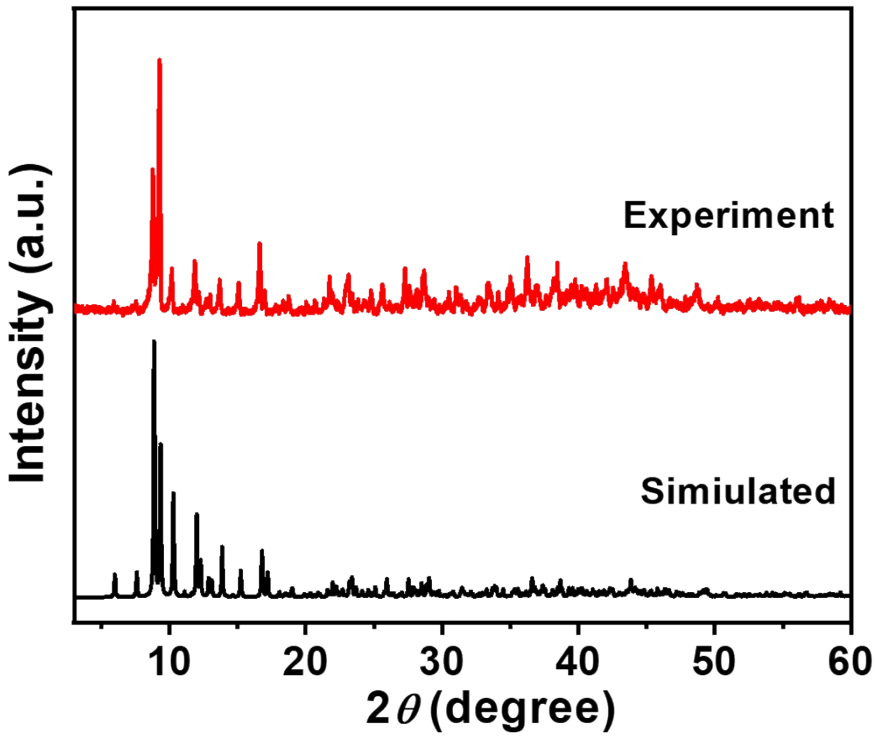

Fig. S2 The PXRD patterns of simulated and experiment of $(NEt_4)_2Mo^{IV}_3S_7Br_6$.

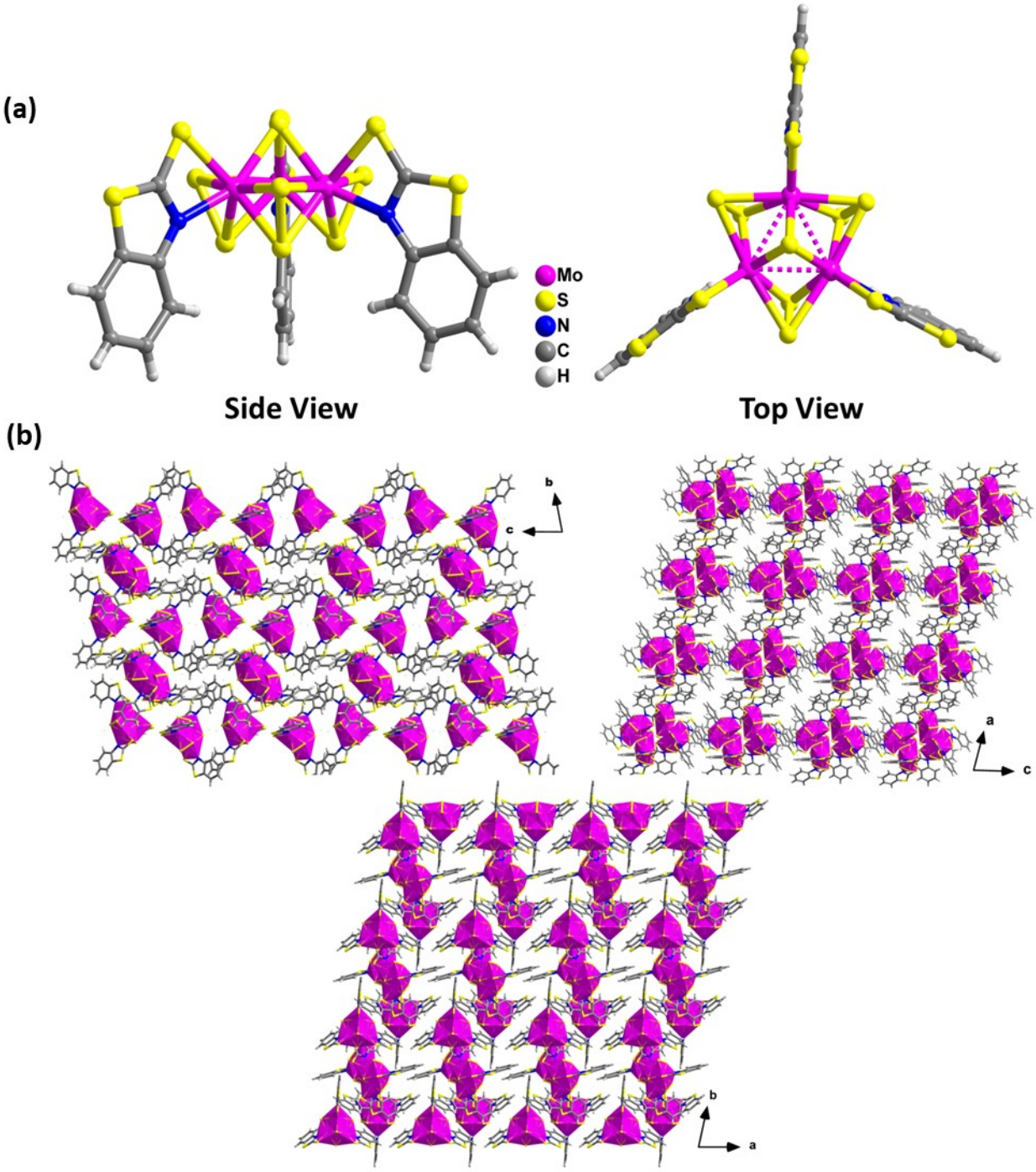

Fig. S3 (a) The crystal structure of compound MoS-MBTZ by side and top view; (b) The packing diagrams of compound MoS-MBTZ in the view of *a*-axis, *b*-axis and *c*-axis.

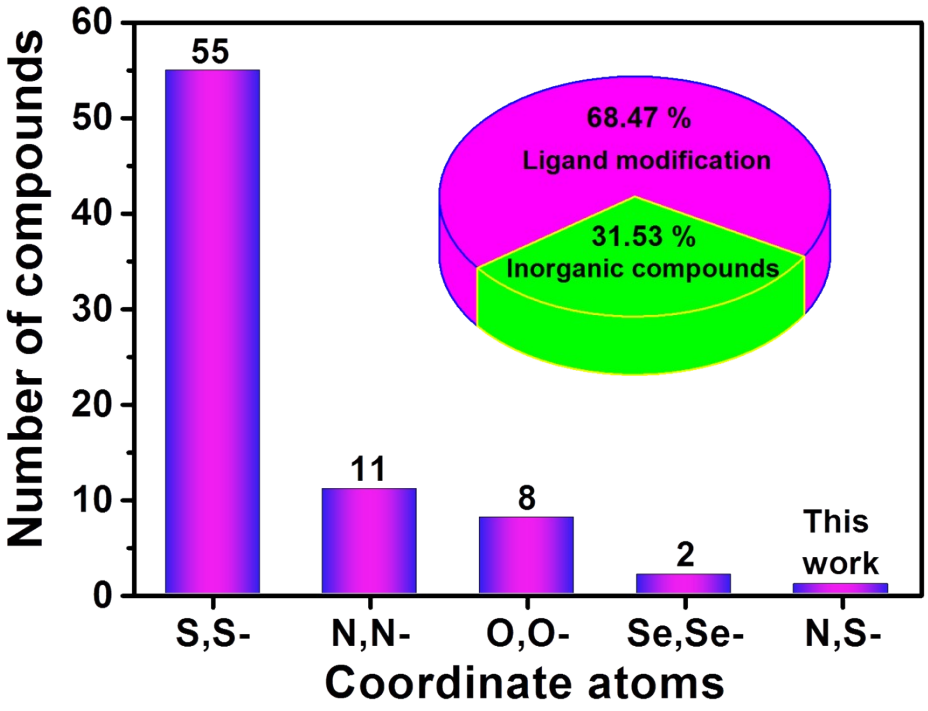

Fig. S4 Summary of compounds with trinuclear [Mo_3S_7] SBUs. All information was surveyed from CCDC database [CSD version 5.42 updates (Sep 2021)].

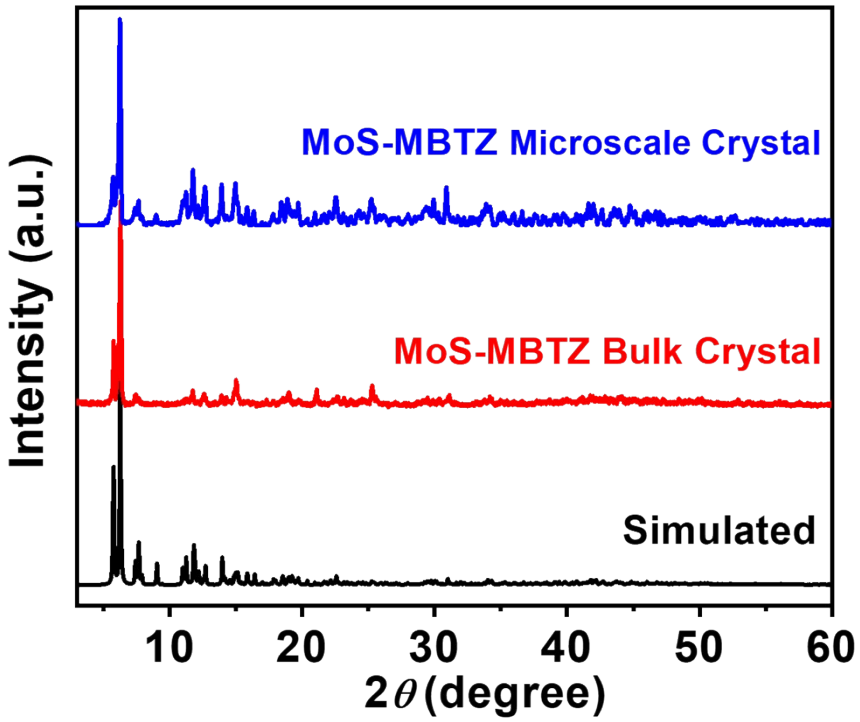

Fig. S5 The PXRD patterns of simulated, MoS-MBTZ bulk crystal and MoS-MBTZ microscale crystal.

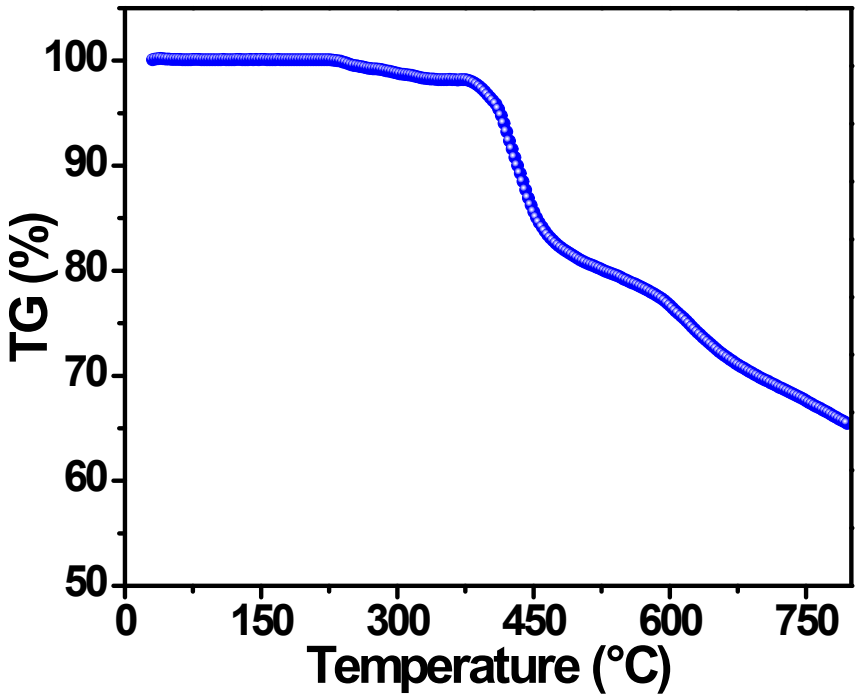

Fig. S6 The TGA curve of MoS-MBTZ.

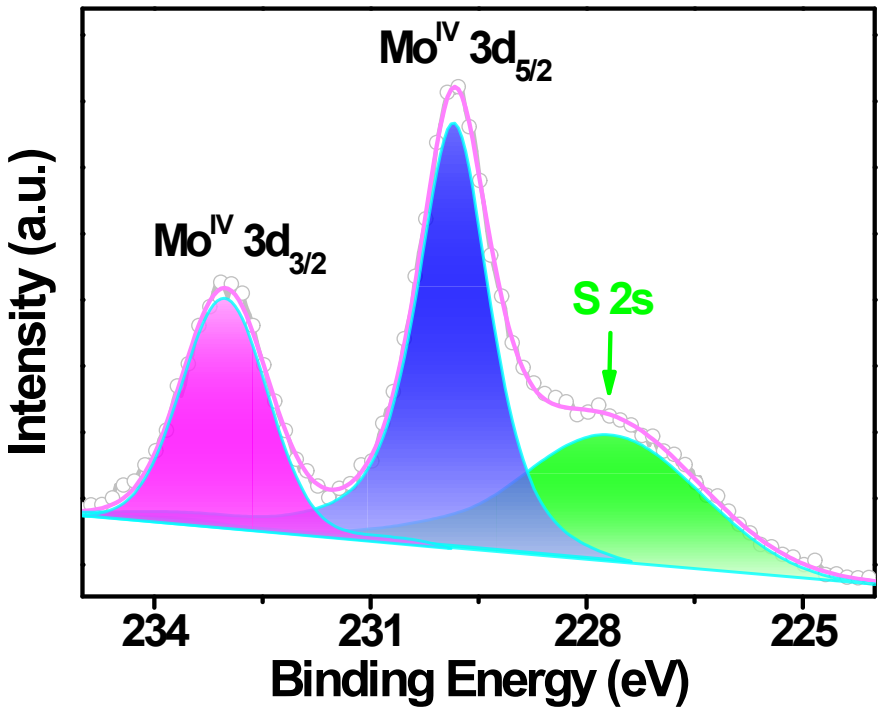

Fig. S7 The high-resolution XPS spectra of Mo 3*d* of compound MoS-MBTZ.

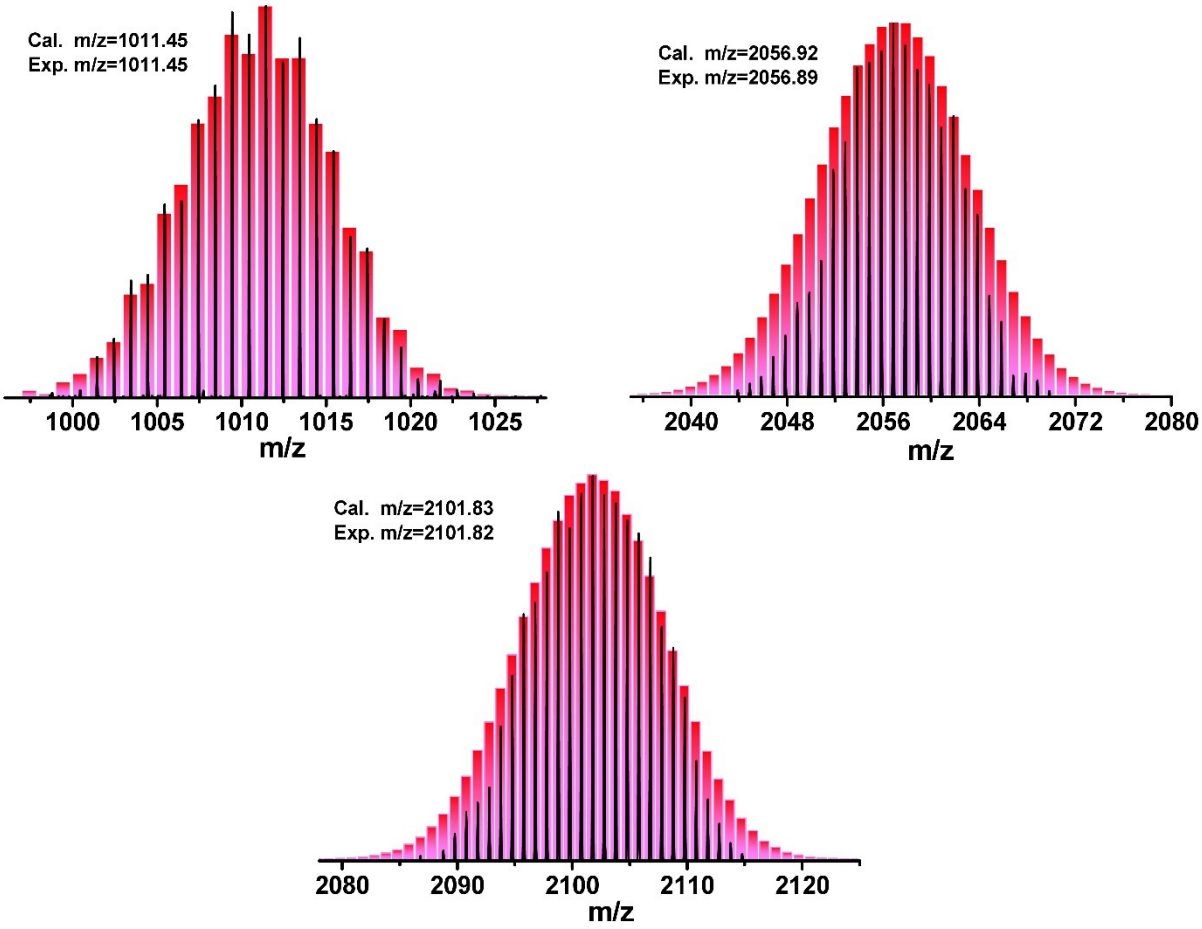

Fig. S8 The experimental and calculated ESI-MS spectra of MoS-MBTZ for $[Mo_3S_7(MBTZ)_3]^+$ (m/z = 1011.45), $\{[Mo_3S_7(MBTZ)_3]_2(OH)(H_2O)\}^+$ (m/z = 2056.89), $\{[Mo_3S_7(MBTZ)_3]_2Br\}^+$ (m/z = 2101.82) fragments .

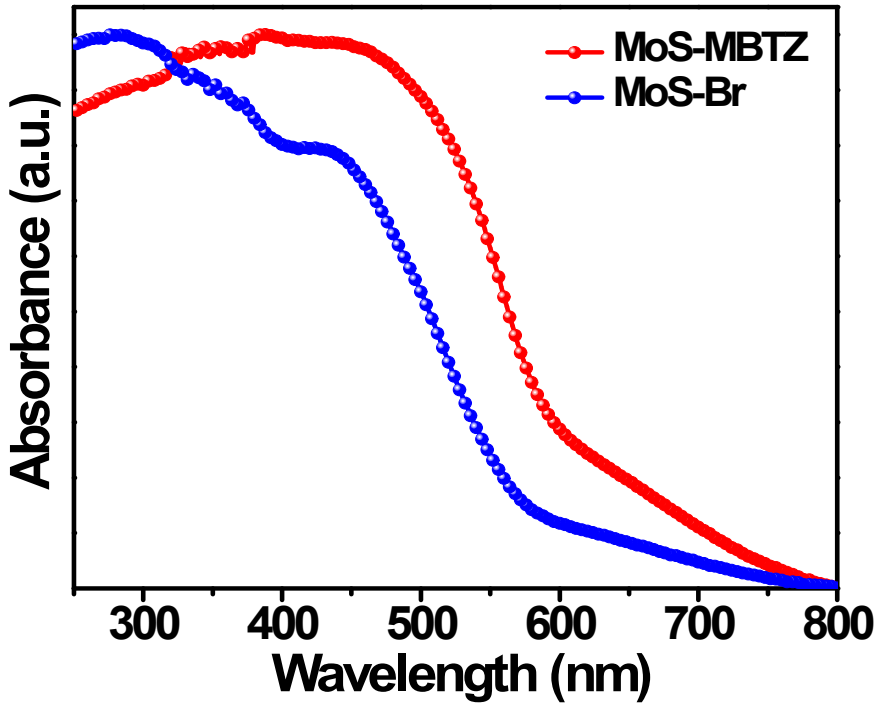

Fig. S9 UV-vis absorption spectra of MoS-MBTZ and MoS-Br.

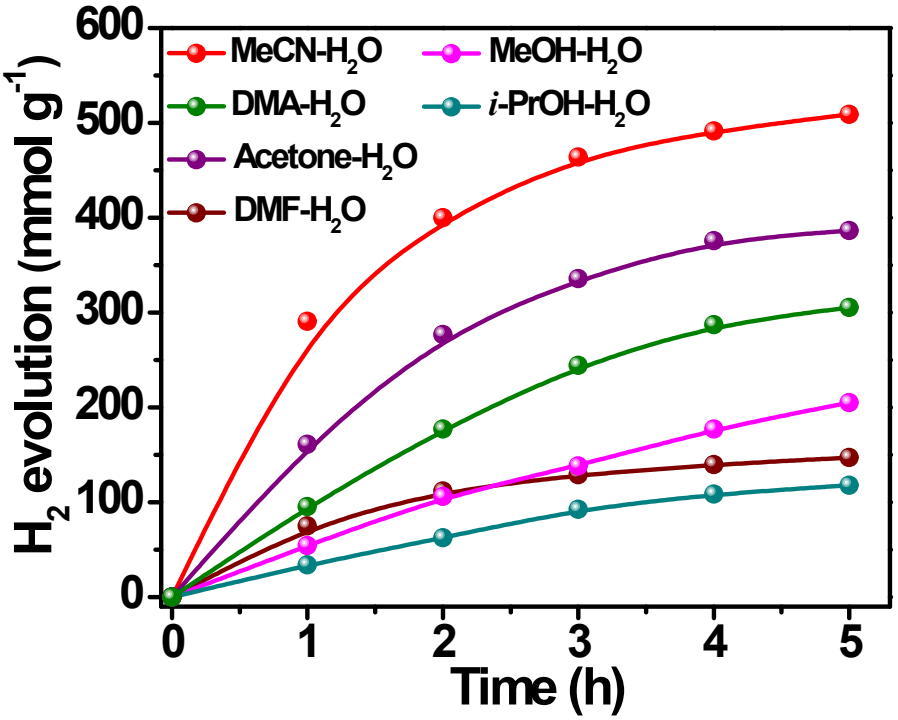

Fig. S10 Photocatalytic H_2 evolution from a mixed solution of organic solvent and H_2O at a volume ratio of 9:1 with $[Ru(bpy)_3]Cl_2$ and TEOA as the photosensitizer and electron donor.

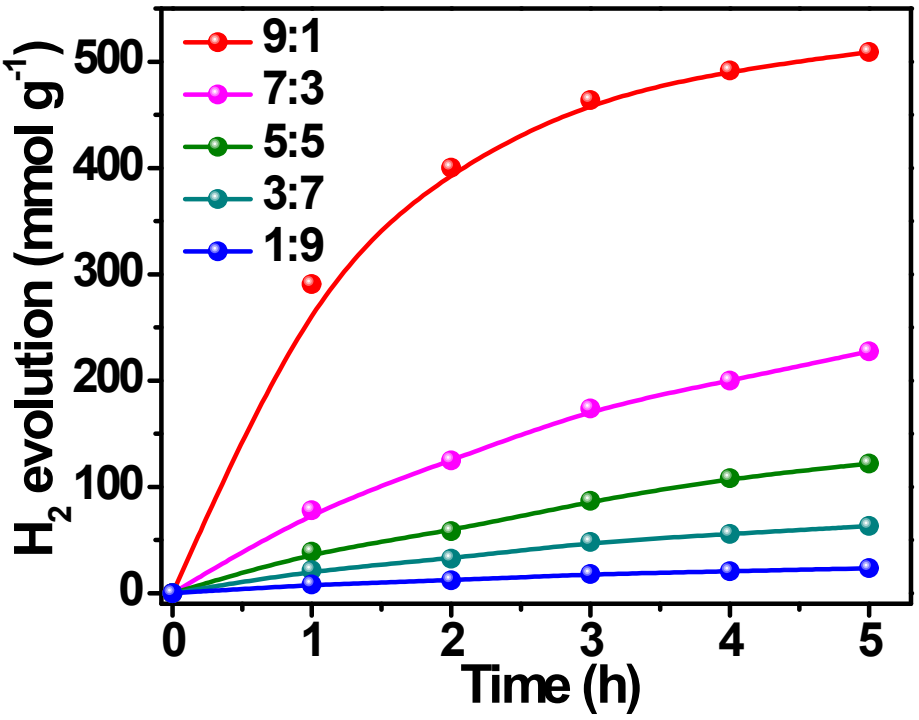

Fig. S11 Photocatalytic H_2 evolution from a mixed solution of CH_3CN and H_2O at different volume ratio with $[Ru(bpy)_3]Cl_2$ and TEOA as the photosensitizer and electron donor.

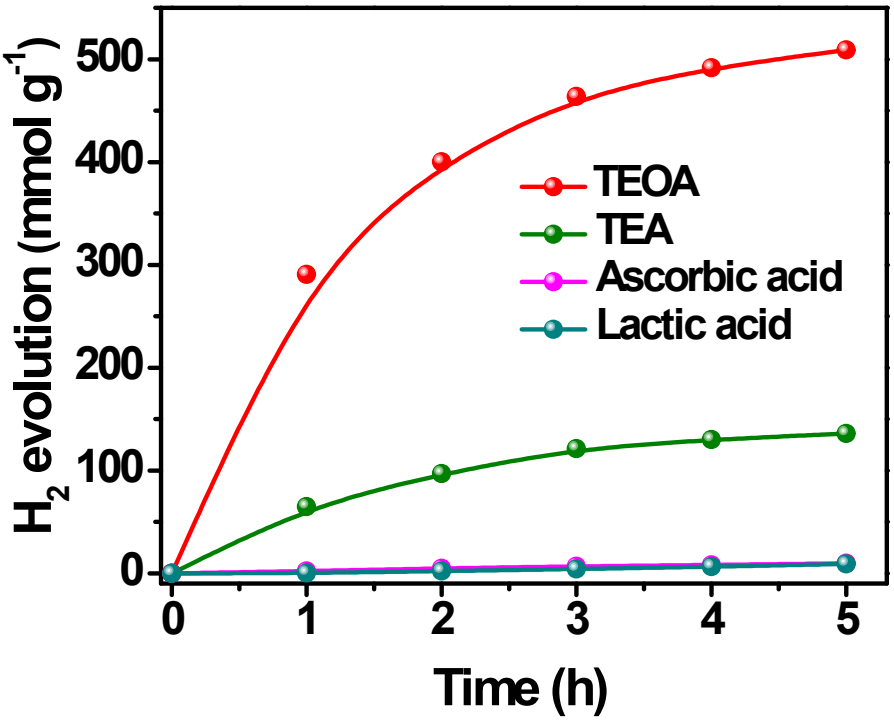

Fig. S12 Photocatalytic H_2 evolution from a mixed solution of CH_3CN and H_2O at a volume ratio of 9:1with different electron donor.

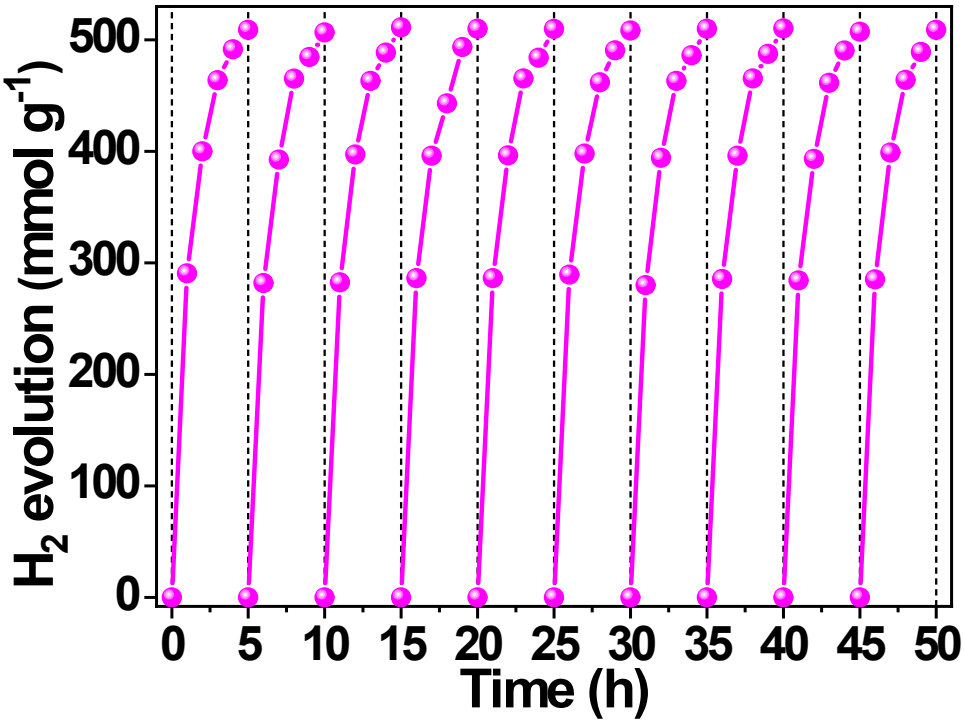

Fig. S13 Photocatalytic H_2 evolution of MoS-MBTZ in recycling experiments.

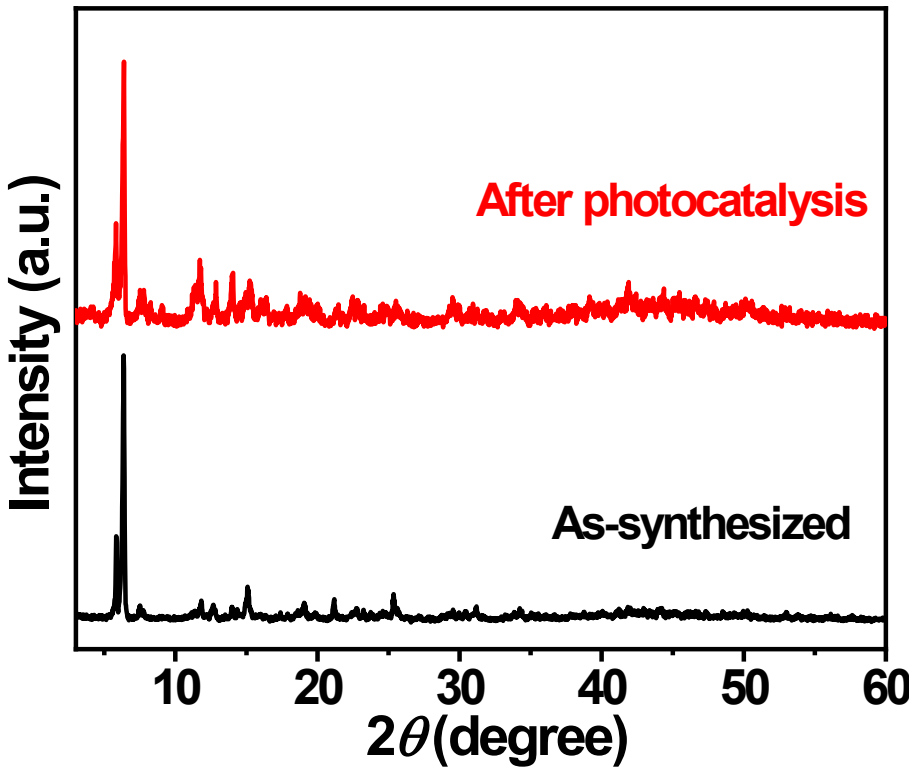

Fig. S14 The XRD of MoS-MBTZ before and after photocatalysis.

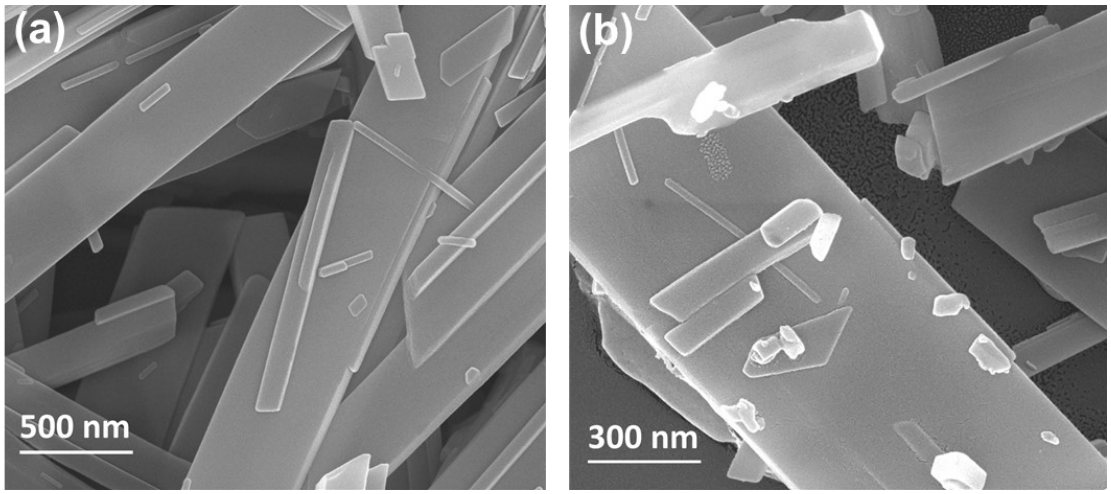

Fig. S15 The SEM image of MoS-MBTZ before (a) and after (b) photocatalysis.

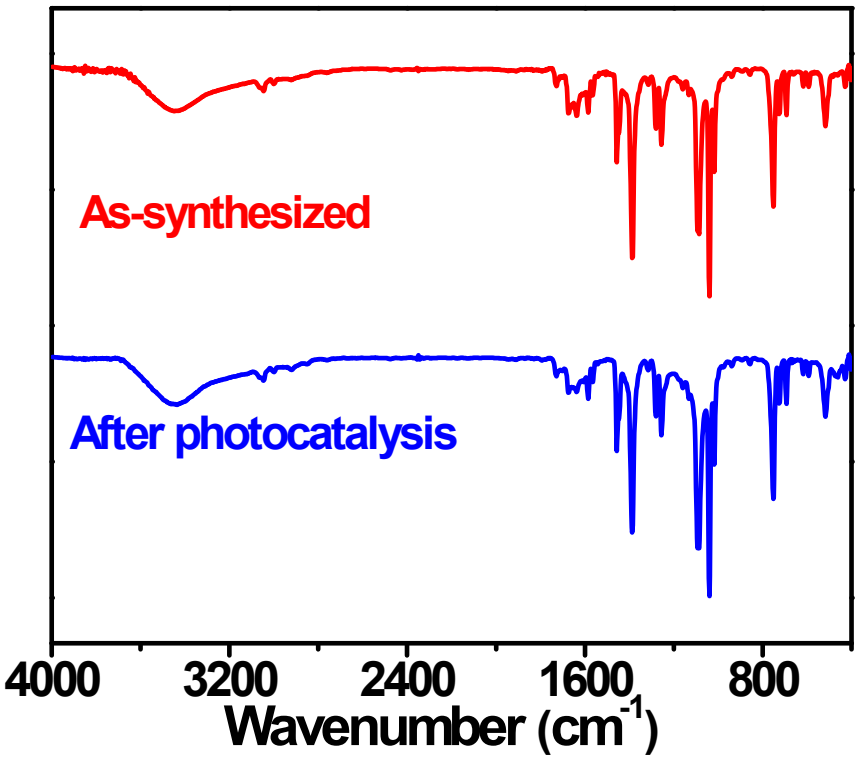

Fig. S16 The FT-IR of MoS-MBTZ before and after photocatalysis.

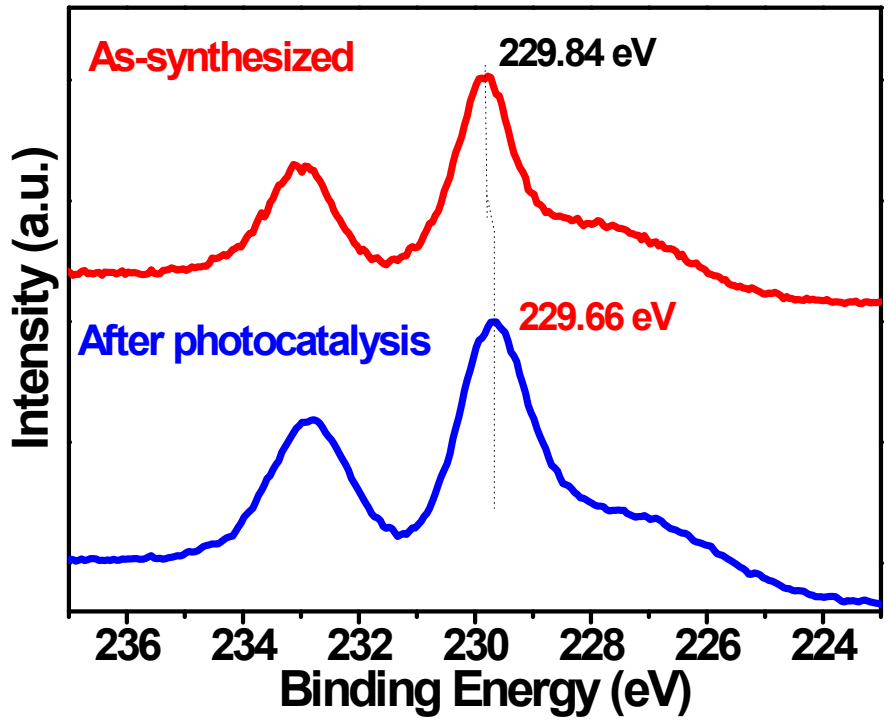

Fig. S17 The XPS image of MoS-MBTZ before and after photocatalysis.

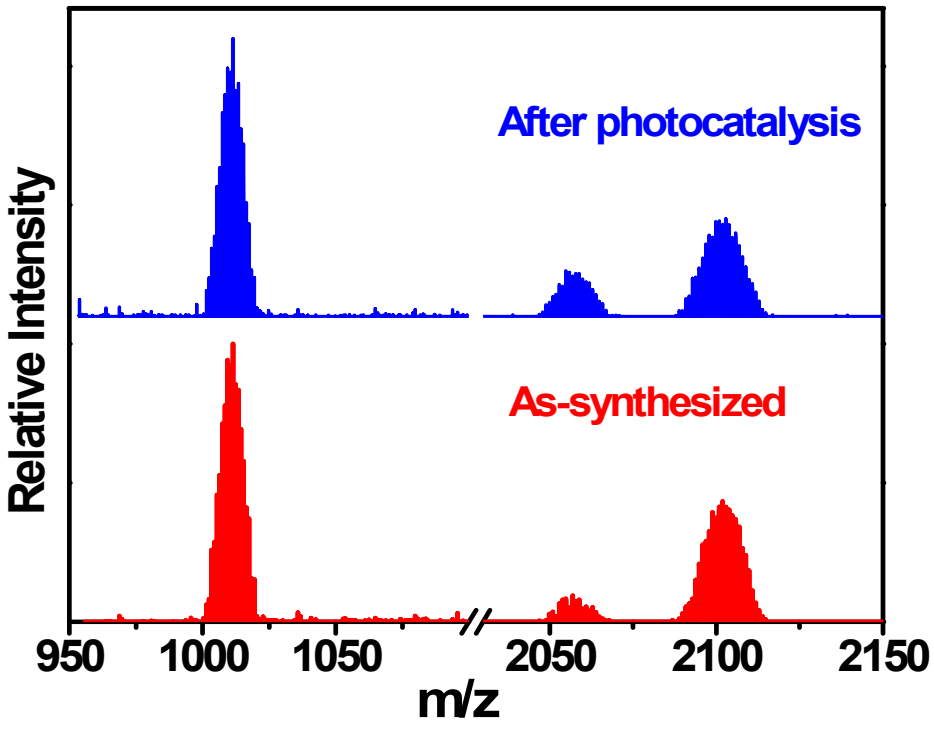

Fig. S18 The ESI-MS of MoS-MBTZ before and after photocatalysis.

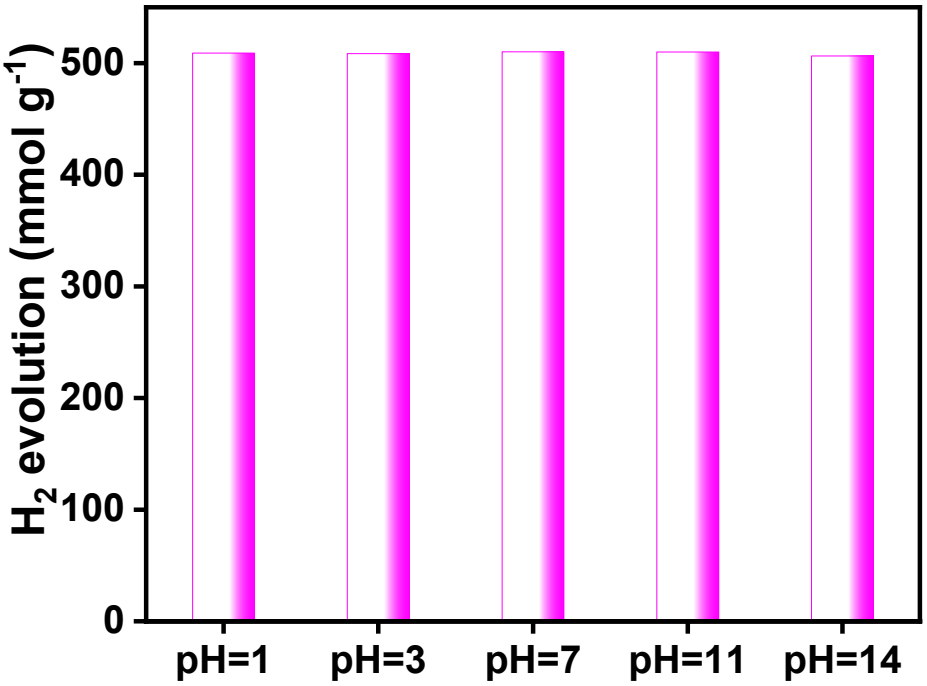

Fig. S19 Photocatalytic H_2 evolution of MoS-MBTZ after soaking in different pH solutions for one month.

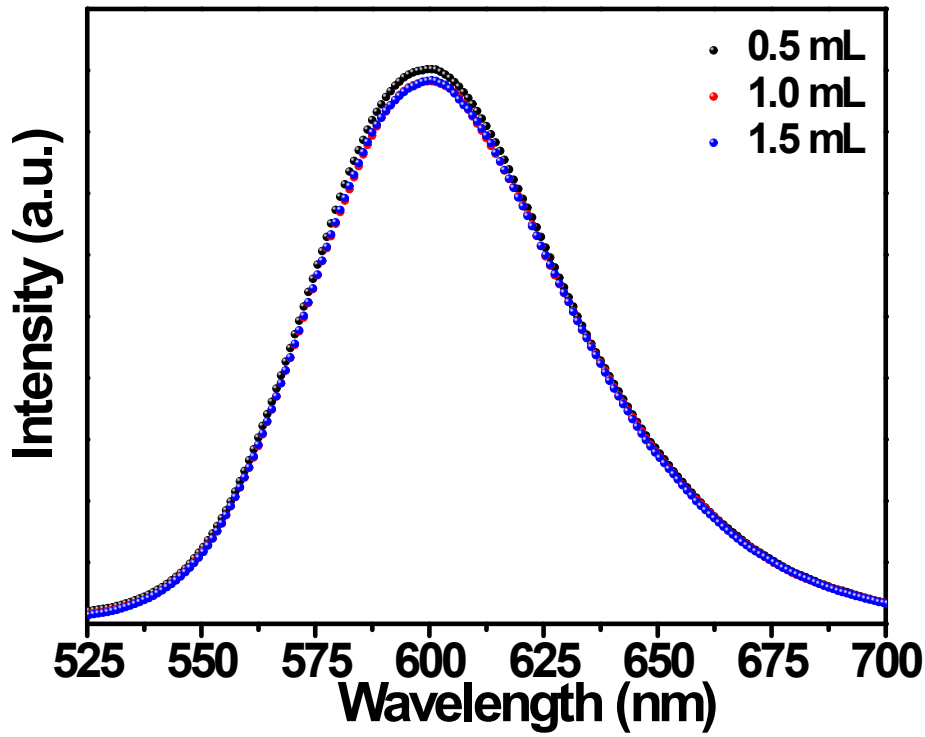

Fig. S20 The steady-state fluorescence spectra of $[Ru(bpy)_3]Cl_2$ upon the addition of increasing amounts of TEOA in the CH_3CN/H_2O solution.

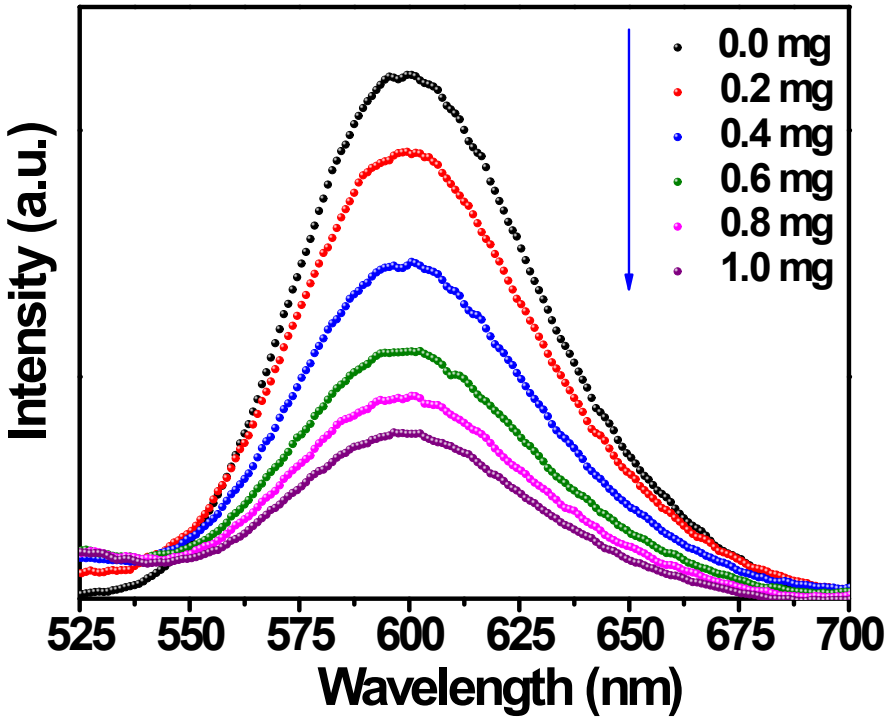

Fig. S21 The steady-state fluorescence spectra of $[Ru(bpy)_3]Cl_2$ upon the addition of increasing amounts of MoS-Br in the CH_3CN/H_2O solution.

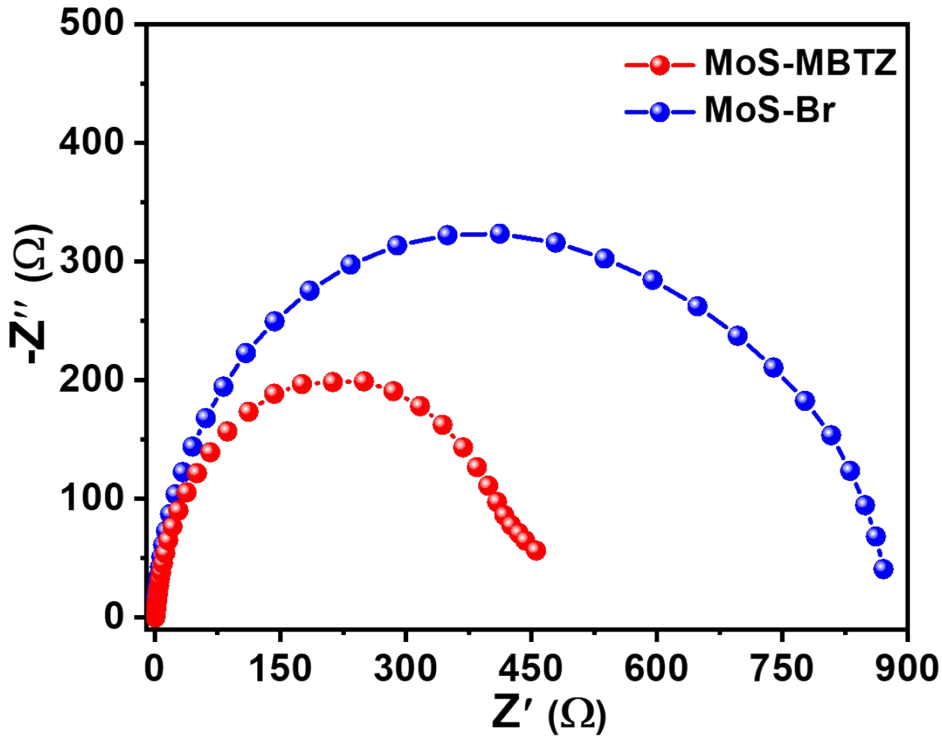

Fig. S22 The EIS Nyquist plots for MoS-MBTZ and MoS-Br.

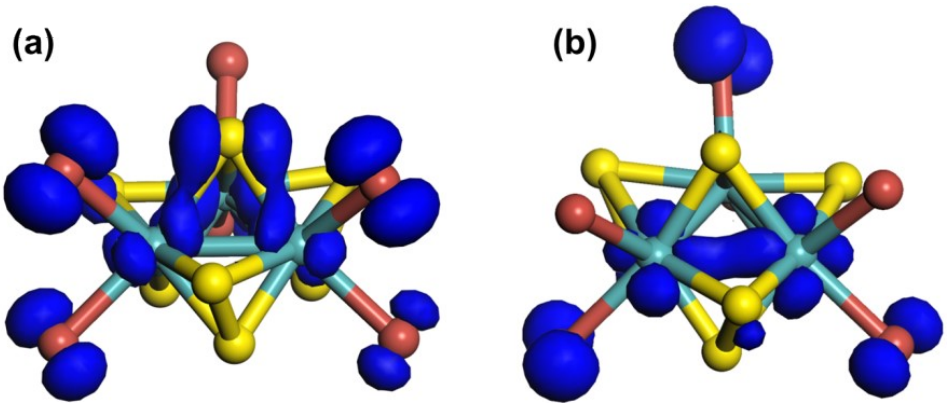

Fig. S23 The molecular orbitals of HOMO (a) and LUMO (b) for MoS-Br.

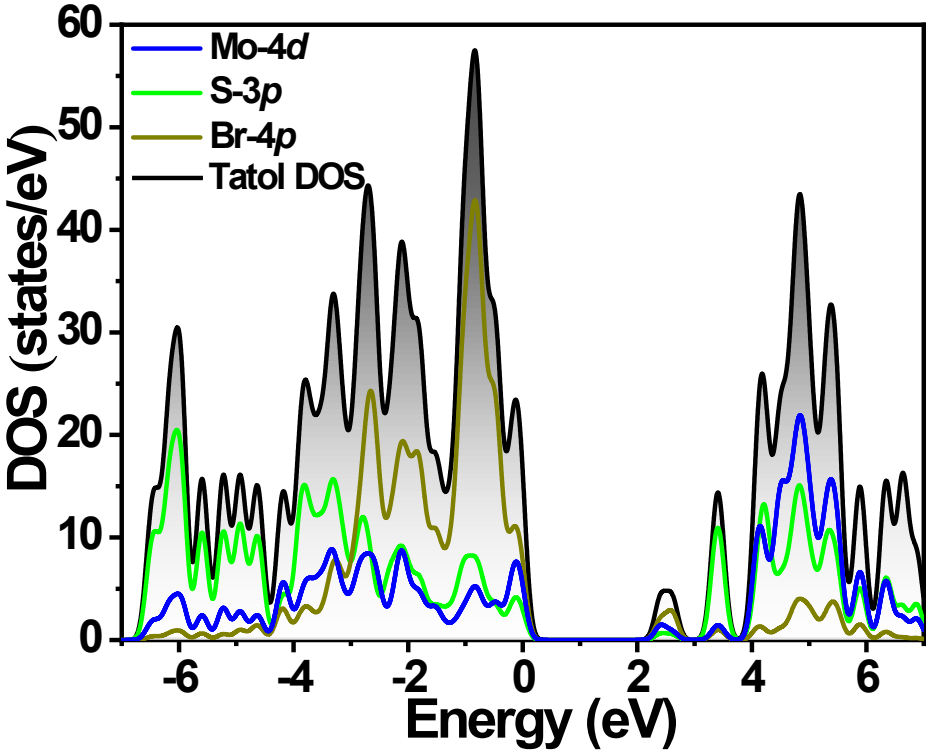

Fig. S24 The PDOS of Mo-4*d*, S-3*p* and Br-4*p* for MoS-Br.

Table S1 Crystallographic data of MoS-MBTZ.

Compound	**MoS-MBTZ**
Formula	$Mo_3S_{13}BrC_{21}H_{12}N_3$
Formula weight	1090.85
T (K)	293
Crystal system	Triclinic
Space group	P-1
a (Å)	15.0168(5)
b (Å)	15.7598(5)
c (Å)	16.2940(5)
α (°)	75.247(3)
β (°)	73.868(3)
γ (°)	74.536(3)
V (Å^3)	3501.7(2)
Z	4
D_c.(g cm^{-3})	2.069
μ (mm^{-1})	3.00
Reflns coll.	12023
Unique reflns	7646
R_{int}	0.072
$^aR_1$ [I ≥ 2σ(I)]	0.061
$^bwR_2$ (all data)	0.159
GOF	0.94

$^aR_1 = \sum||F_o| - |F_c||/\sum|F_o|$, $^bwR_2 = [\sum w(F_o^2 - F_c^2)^2/\sum w(F_o^2)^2]^{1/2}$.

Table S2 Selected bond lengths (Å) and angles (°) of MoS-MBTZ.

Mo1-Mo2	2.6958 (11)	Mo4-Mo5	2.6974 (12)
Mo1-Mo3	2.6978 (11)	Mo4-Mo6	2.6991 (14)
Mo1-S1	2.363 (2)	Mo4-S14	2.362 (3)
Mo1-S2	2.473 (2)	Mo4-S15	2.470 (3)
Mo1-S3	2.406 (2)	Mo4-S16	2.402 (3)
Mo1-S6	2.475 (2)	Mo4-S17	2.466 (3)
Mo1-S7	2.394 (3)	Mo4-S18	2.397 (3)
Mo1-S8	2.500 (3)	Mo4-S21	2.513 (3)
Mo1-N1	2.171 (7)	Mo4-N4	2.197 (9)
Mo2-Mo3	2.7034 (10)	Mo5-Mo6	2.7029 (12)
Mo2-S1	2.362 (2)	Mo5-S14	2.361 (3)
Mo2-S2	2.475 (3)	Mo5-S17	2.475 (3)
Mo2-S3	2.402 (2)	Mo5-S18	2.409 (3)
Mo2-S4	2.472 (3)	Mo5-S19	2.475 (3)
Mo2-S5	2.400 (3)	Mo5-S20	2.413 (3)
Mo2-S10	2.509 (3)	Mo5-S23	2.490 (3)
Mo2-N2	2.184 (7)	Mo5-N5	2.183 (8)
Mo3-S1	2.373 (3)	Mo6-S14	2.364 (3)
Mo3-S4	2.483 (3)	Mo6-S15	2.479 (3)
Mo3-S5	2.402 (3)	Mo6-S16	2.412 (3)
Mo3-S6	2.470 (3)	Mo6-S19	2.465 (3)
Mo3-S7	2.398 (2)	Mo6-S20	2.414 (3)
Mo3-S12	2.521 (3)	Mo6-S25	2.509 (3)
Mo3-N3	2.176 (8)	Mo6-N6	2.187 (8)
S1-Mo1-S2	84.99 (8)	S14-Mo4-S15	84.98 (10)
S1-Mo1-S3	110.33 (8)	S14-Mo4-S16	110.58 (10)
S1-Mo1-S6	86.35 (8)	S14-Mo4-S17	86.48 (10)
S1-Mo1-S7	110.82 (9)	S14-Mo4-S18	110.81 (9)
S1-Mo1-S8	86.81 (9)	S14-Mo4-S21	86.84 (11)
S2-Mo1-S6	171.33 (9)	S15-Mo4-S21	91.84 (11)
S2-Mo1-S8	90.89 (9)	S16-Mo4-S15	49.91 (10)
S3-Mo1-S2	49.81 (8)	S16-Mo4-S17	134.00 (10)
S3-Mo1-S6	133.90 (9)	S16-Mo4-S21	133.57 (10)
S3-Mo1-S8	132.82 (9)	S17-Mo4-S15	171.46 (11)
S6-Mo1-S8	89.11 (9)	S17-Mo4-S21	87.95 (10)
S7-Mo1-S2	133.80 (9)	S18-Mo4-S15	133.85 (10)
S7-Mo1-S3	84.28 (9)	S18-Mo4-S16	84.26 (10)

S7-Mo1-S6	49.82 (9)	S18-Mo4-S17	49.89 (9)
S7-Mo1-S8	131.55 (9)	S18-Mo4-S21	130.63 (11)
N1-Mo1-S1	152.1 (2)	N4-Mo4-S14	151.7 (3)
N1-Mo1-S2	92.7 (2)	N4-Mo4-S15	95.4 (3)
N1-Mo1-S3	88.6 (2)	N4-Mo4-S16	90.4 (3)
N1-Mo1-S6	95.2 (2)	N4-Mo4-S17	92.2 (3)
N1-Mo1-S7	90.8 (2)	N4-Mo4-S18	89.2 (3)
N1-Mo1-S8	65.4 (2)	N4-Mo4-S21	64.9 (3)
S3-Mo2-S2	49.83 (9)	S14-Mo5-S17	86.31 (10)
S1-Mo2-S3	110.52 (9)	S14-Mo5-S18	110.43 (10)
S1-Mo2-S4	84.77 (9)	S14-Mo5-S19	84.95 (10)
S1-Mo2-S5	110.40 (9)	S14-Mo5-S20	110.44 (10)
S1-Mo2-S10	87.42 (8)	S14-Mo5-S23	85.44 (9)
S2-Mo2-S10	88.49 (9)	S17-Mo5-S19	171.17 (10)
S3-Mo2-Mo1	55.96 (6)	S17-Mo5-S23	89.57 (10)
S3-Mo2-S4	135.74 (9)	S18-Mo5-S17	49.67 (9)
S3-Mo2-S10	130.20 (9)	S18-Mo5-S19	133.21 (9)
S4-Mo2-S2	169.71 (9)	S18-Mo5-S20	84.13 (10)
S4-Mo2-S10	90.27 (9)	S18-Mo5-S23	132.70 (11)
S19-Mo5-S23	90.98 (10)	S20-Mo5-S17	133.64 (10)
S5-Mo2-S2	135.81 (9)	S20-Mo5-S19	49.47 (9)
S5-Mo2-S3	86.29 (9)	S20-Mo5-S23	133.11 (11)
S5-Mo2-S4	49.77 (9)	N5-Mo5-S14	150.2 (2)
S5-Mo2-S10	131.73 (10)	N5-Mo5-S17	86.8 (2)
N2-Mo2-S1	153.7 (2)	N5-Mo5-S18	86.5 (2)
N2-Mo2-S2	94.8 (2)	N2-Mo2-S4	94.1 (2)
N2-Mo2-S3	88.6 (2)	N5-Mo5-S19	101.4 (2)
N2-Mo2-S5	88.0 (2)	N5-Mo5-S20	95.1 (2)
N2-Mo2-S10	66.3 (2)	N5-Mo5-S23	65.5 (2)
S1-Mo3-S4	84.30 (9)	S14-Mo6-S15	84.75 (9)
S1-Mo3-S5	109.92 (8)	S14-Mo6-S16	110.16 (10)
S1-Mo3-S6	86.23 (9)	S14-Mo6-S19	85.11 (9)
S1-Mo3-S7	110.34 (9)	S14-Mo6-S20	110.31 (9)
S1-Mo3-S12	88.40 (9)	S14-Mo6-S25	86.76 (10)
S4-Mo3-S12	91.84 (9)	S15-Mo6-S25	88.51 (10)
S5-Mo3-S4	49.62 (8)	S16-Mo6-S15	49.70 (10)
S5-Mo3-S6	134.63 (9)	S16-Mo6-S19	135.38 (10)
S5-Mo3-S12	132.60 (10)	S16-Mo6-S20	86.11 (10)
S6-Mo3-S4	170.53 (9)	S16-Mo6-S25	130.54 (10)

S6-Mo3-S12	88.19 (9)	S19-Mo6-S15	169.86 (10)
S7-Mo3-S4	134.19 (9)	S19-Mo6-S25	90.59 (10)
S7-Mo3-S5	84.98 (9)	S20-Mo6-S15	135.48 (11)
S7-Mo3-S6	49.83 (9)	S20-Mo6-S19	49.58 (9)
S7-Mo3-S12	130.23 (9)	S20-Mo6-S25	132.39 (11)
N3-Mo3-S1	154.0 (2)	N6-Mo6-S14	152.7 (2)
N3-Mo3-S4	97.0 (2)	N6-Mo6-S15	90.9 (2)
N3-Mo3-S5	89.9 (2)	N6-Mo6-S16	86.7 (2)
N3-Mo3-S6	91.7 (2)	N6-Mo6-S19	98.0 (2)
N3-Mo3-S7	87.4 (2)	N6-Mo6-S20	91.6 (2)
N3-Mo3-S12	65.6 (2)	N6-Mo6-S25	66.2 (2)

Table S3 Photocatalytic H_2 evolution from a mixed solution of different organic solvent and H_2O at a volume ratio of 9:1.

Solvent system	H_2 evolution Rate (mmol g^{-1})	υ (H_2) (mmol g^{-1} h^{-1})
CH_3CN-H_2O	509.04	101.81
DMF-H_2O	147.03	29.41
MeOH-H_2O	205.16	41.02
i-PrOH-H_2O	117.84	23.57
Acetone-H_2O	386.55	77.31
DMA-H_2O	305.18	61.04

Table S4 Photocatalytic H_2 evolution from a mixed solution of CH_3CN and H_2O at a different volume ratio.

Solvent volume ratio	H_2 evolution Rate (mmol g^{-1})	υ (H_2) (mmol g^{-1} h^{-1})
9:1	509.04	101.81
7:3	227.43	45.49
5:5	121.75	24.35
3:7	63.09	12.62
1:9	23.30	4.66

Table S5 Photocatalytic H_2 evolution from a mixed solution of CH_3CN and H_2O at a volume ratio of 9:1with different electron donor.

Electron donor	H_2 evolution Rate (mmol g^{-1})	υ (H_2) (mmol g^{-1} h^{-1})
TEOA	509.04	101.81
TEA	135.81	27.16
Ascorbic acid	9.55	1.91
Lactic acid	9.04	1.81

Table S6 Summary of Mo-S clusters or MoS_2-based photocatalysts for H_2 evolution of water splitting.

Catalyst	Photosensitizer or co-catalyst	Light source	HER Rate (μmol g^{-1} h^{-1})	Ref.
MoS-MBTZ	**$Ru(bpy)_3Cl_2$**	**≥420 nm**	**101800**	**This work**
Mo_3S_{13}@EB-COF	$Ru(bpy)_3Cl_2$	≥420 nm	13215	4
$[Mo_3S_{13}]^{2-}$	$Ru(bpy)_3Cl_2$	≥420 nm	28860	5
$[Mo_3S_7(S_2CNEt_2)_3]I$	$Ru(bpy)_3Cl_2$	LEDs, 460 nm	184.5	6
SiW_{12}-$[Mo_3S_{13}]^{2-}$	SiW_{12}	350-780 nm	1395	7
MoS_2/PyP(IM)	PyP	≥420 nm	540	8
MoS_2/TiO_2	-	365 nm	2443	9
$Ti_3C_2(TiO_2)$@CdS/MoS_2	-	≥420 nm	8470	10
$MoS_2/ZnIn_2S_4$	-	≥420 nm	3891.6	11
g-C_3N_4/MoS_2 nanodot	-	≥420 nm	660	12
1T-MoS_2/O-g-C_3N_4	-	≥420 nm	1841.7	13
TiO_2@MoS_2	-	≥420 nm	7571	14
e-MoS_2–Au_{CNC}–CdS	-	≥420 nm	237.9	15
1T-MoS_2/P25/NiO_x	-	≥420 nm	16291	16

Table S7 Control photocatalytic experiments using MoS-MBTZ as catalyst.

Entry	Control Conditions	H_2 evolution Rate (mmol g^{-1})	υ (H_2) (mmol g^{-1} h^{-1})
1	Without MoS-MBTZ	28.56	3.81
2	Without $[Ru(bpy)_3]Cl_2$	15.82	1.58
3	Without TEOA	4.50	0.18
4	Without light	5.03	0.21
5	MoS-MBTZ	545.21	101.80

References

[1] Z. Ji, C. Trickett, X. Pei, O. M. Yaghi, *J. Am. Chem. Soc.* **2018**, *140*, 13618-13622.

[2] G. M. Sheldrick, SHELXT-Integrated Space-Group and Crystal-Structure Determination, *Acta Cryst.*, 2015, **A71**, 3-8.

[3] M. D. Segall, P. J. D. Lindan, M. J. Probert, C. J. Pickard, P. J. Hasnip, S. J. Clark, M. C. Payne, *J. Phys. Condens. Matter.* 2002, **14**, 2717.

[4] Y.-J. Cheng, R. Wang, S. Wang, X.-J. Xi, L.-F. Ma and S.-Q. Zang, *Chem. Commun*., 2018, **54**, 13563-13566.

[5] Y. Lei, M. Yang, J. Hou, F. Wang, E. Cui, C. Kong and S. Min, *Chem. Commun*., 2018, **54**, 603-606.

[6] P. R. Fontenot, B. Shan, B. Wang, S. Simpson, G. Ragunathan, A. F. Greene, A. Obanda, L. A. Hunt, N. I. Hammer, C. E. Webster, J. T. Mague, R. H. Schmehl and J. P. Donahue, *Inorg. Chem*., 2019, **58**, 16458-16474.

[7] W. Li, S. Min, F. Wang, Z. Zhang and D. Gao, *Chem. Commun*., 2021, **57**, 1121-1124.

[8] S. Zang, G. Zhang, Z.-A. Lan, D. Zheng and X. Wang, *Appl. Catal. B-Environ.,* 2019, **251**, 102-111.

[9] W. Wang, S. Zhu, Y. Cao, Y. Tao, X. Li, D. Pan, D. L. Phillips, D. Zhang, M. Chen, G. Li and H. Li, *Adv. Funct. Mater.*, 2019, **29**, 1901958.

[10] Z. Ai, Y. Shao, B. Chang, B. Huang, Y. Wu and X. Hao, *Appl. Catal. B-Environ.*, 2019, **242**, 202-208.

[11] Z. Zhang, L. Huang, J. Zhang, F. Wang, Y. Xie, X. Shang, Y. Gu, H. Zhao and X. Wang, *Appl. Catal. B-Environ.*, 2018, **233**, 112-119.

[12] X. Shi, M. Fujitsuka, S. Kim and T. Majima, *Small*, 2018, **14**, 1703277.

[13] H. Xu, J. Yi, X. She, Q. Liu, L. Song, S. Chen, Y. Yang, Y. Song, R. Vajtai, J. Lou, H. Li, S. Yuan, J. Wu and P. M. Ajayan, *Appl. Catal. B-Environ.* 2018, **220**, 379-385.

[14] L. Wang, X. Liu, J. Luo, X. Duan, J. Crittenden, C. Liu, S. Zhang, Y. Pei, Y. Zeng and X. Duan, *Angew. Chem. Int. Ed.* 2017, **56**, 7610-7614.

[15] D. H. Wi, S. Y. Park, S. Lee, J. Sung, J. W. Hong and S. Woo Han, *J. Mater. Chem. A*, 2018, **6**, 13225-13235.

[16] H. Lin, K. Zhang, G. Yang, Y. Li, X. Liu, K. Chang, Y. Xuan, J. Ye, *Appl. Catal. B-Environ.*, 2020, **279**, 119387.